Available online at www.sciencedirect.com
ScienceDirect
International Journal of Thermal Sciences 46 (2007) 1172–1181
International Journal of Thermal Sciences
www.elsevier.com/locate/ijts

Heat transfer mechanism and flow pattern during flow boiling of water in a vertical narrow channel—experimental results

Ewelina Sobierska *, Rudi Kulenovic, Rainer Mertz

Institute of Nuclear Technology and Energy Systems, University of Stuttgart, Pfaffenwaldring 31, 70569 Stuttgart, Germany

Received 1 August 2006; received in revised form 20 June 2007; accepted 20 June 2007

Abstract

Experimental investigations on flow boiling phenomena in a vertical narrow rectangular microchannel with the hydraulic diameter $d_h = 0.48$ mm were carried out. The experiments were performed under fluid-inlet subcooled conditions with de-ionised and degassed water for different mass fluxes. Investigations on pressure drop and heat transfer during single- and two-phase flow have been carried out. Moreover, flow visualisation of the two-phase flow patterns along the channel was performed using a digital high-speed video camera.

The present work outlines local heat transfer coefficients for three mass fluxes (200, 700 and 1500 kg m^{-2} s^{-1}) and heat fluxes (30–110, 35–150 and 65–200 kW m^{-2}) during two-phase flow. The visual observations were used to obtain a better insight about the heat transfer mechanisms. The goal of this work is to find the circumstance of the best heat transfer circumstance in microchannels.

Keywords: Micro channel; Heat transfer; Visualisation; Flow boiling

1. Introduction

The mechanism of flow boiling in narrow channels is complicated due to the fact that with a change of flow patterns simultaneously different vaporisation mechanisms may encounter at different positions along such channels. The boiling of refrigerants in small-diameter channels can be dominated by nucleate boiling, by convective boiling, or both mechanisms. Near to the onset of boiling the nucleation mechanism usually dominates. With increasing vapour quality the flow regime undergoes a transition to an annular or nearly annular flow. Then the film vaporisation (convective boiling) becomes a considerable heat transfer mechanism and can even suppress completely the nucleate boiling. Because of vaporisation the liquid film may completely disappear (dryout) or only at some channel positions (partial dryout). As a result the heat transfer coefficient increases along the channel up to a certain position where partial dryout starts to occur. After it the heat transfer coefficient (average value around the channel perimeter) decreases continuously with the decrease of the wetted part of the channel wall [1].

Diaz et al. [2] investigated the flow boiling of water and hydrocarbons (*n*-hexane, *n*-heptane, *n*-octane and a mixture *n*-hexane/*n*-heptane) in circular tubes ($d_h = 1.5$ mm) and rectangular channels (height = 0.3–0.7 mm, width = 10 mm, $d_h =$ 0.58–1.31 mm). For pure hydrocarbons, it was observed that the heat transfer coefficient has a maximum value in the initial region indicating a dominance of nucleate boiling. Then the heat transfer coefficient decreases along the channel axis with increasing vapour quality. This behaviour was explained by "steam-influenced boiling" characterised by increasing partial dryouts. However, for water and hydrocarbon mixtures a rise of the heat transfer coefficient was observed with increasing vapour quality after an initial region with locally dominating nucleate boiling. This increase is typical for convective boiling. The same tendency was observed by Lin et al. [3] for water in a tube with hydraulic diameter 1.1 mm at moderate heat fluxes. For heat fluxes greater than 60 kW m^{-2}, the heat transfer coefficient decreases. The authors argued that nucleate boiling is dominant at these heat fluxes, and furthermore the decrease of the heat transfer coefficient with increasing vapour quality is a consequence of the linear pressure drop assumption from onset

* Corresponding author. Tel.: +49 711 685 62454; fax: +49 711 685 62010.
E-mail address: ewelina.sobierska@ike.uni-stuttgart.de (E. Sobierska).

1290-0729/$ – see front matter © 2007 Published by Elsevier Masson SAS.
doi:10.1016/j.ijthermalsci.2007.06.011

Nomenclature

A	heat transfer area	m^2	
A_{sect}	area of channel cross-section	m^2	
Bo	Boiling number, $Bo = q/(G\Delta h_{LG})$		
Co^*	Confinement number, $Co^* = [g(\rho_L - \rho_G)d_h^2/\sigma]^{-0.5}$		
C_0	distribution parameter defined by Eq. (11)		
C_p	specific heat capacity	$J\,kg^{-1}\,K^{-1}$	
d_h	hydraulic diameter, $d_h = 4W \cdot H/[2(W + H)]$	m	
G	mass flux	$kg\,m^{-2}\,s^{-1}$	
g	gravitational acceleration	$m\,s^{-2}$	
H	depth of channel	m	
h	heat transfer coefficient	$W\,m^{-2}\,K^{-1}$	
Δh_{LG}	latent heat of vaporisation	$J\,kg^{-1}$	
i	specific enthalpy	$J\,kg^{-1}$	
j	superficial velocity	$m\,s^{-1}$	
L	length	m	
$N_{\mu L}$	viscosity number		
p	pressure	Pa	
Q	heat flow rate	W	
q	heat flux	$W\,m^{-2}$	
Re	Reynolds number		
S	heated perimeter of channel, $S = W + 2H$	m	
T	temperature	K	
V	volumetric flow rate	$m^3\,s^{-1}$	
W	width of channel	m	
X_{tt}	Martinelli parameter		
x_{th}	thermodynamic vapour quality		
Z	distance from inlet	m	

Greek symbols

α	void fraction	
λ	thermal conductivity	$W\,m^{-1}\,K^{-1}$
μ	dynamic viscosity	Pa s
ρ	density	$kg\,m^{-3}$
σ	surface tension	$N\,m^{-1}$

Subscripts

ave	average
G	gas
in	inlet
L	liquid
loss	loss
ONB	onset of boiling
sat	saturation
vb	vapour body
W	wall

of boiling and hence a consequence of the heat transfer coefficient definition.

Agostini and Bontemps [4] investigated flow boiling of R134a in rectangular multichannels ($d_h = 2.01$ mm). They observed a weak influence of the vapour quality on the heat transfer coefficient for Boiling number $Bo \geqslant 4.3 \cdot 10^{-4}$ and vapour quality $x \leqslant 0.4$. Thus, the nucleate boiling regime determines this region. For the same Boiling number but vapour quality greater than 0.4, the heat transfer coefficient decreases with the rising vapour quality. This indicates that a partial dryout occurs because of a vapour body confinement thinning the liquid layer thickness at the tube wall. For $Bo \leqslant 4.3 \cdot 10^{-4}$, the heat transfer coefficient is weakly dependent on the vapour quality up to a transition value. Then it starts to increase. This behaviour may correspond to a competition between convective boiling and flow regimes where a partial dryout and a regeneration of the liquid layer occur. Based on this observations, the transition from nucleate boiling to supposed convective boiling occurs at $Bo(1 - x) \approx 2.2 \cdot 10^{-4}$ regardless of the heat and mass flux.

A review about the boiling behaviour of refrigerants in small pipes was presented by Vlasie et al. [5] which can be summarised that boiling can be dominated by nucleate as well as convective boiling or by both mechanisms. The boundary between nucleate and convective boiling as a function of the wall superheat proposed by Tran et al. [6] appears to be successful in reconciling the different trends observed by various researchers. Correlations based on the nucleate boiling mechanism work mostly satisfactory for boiling of pure fluids in small diameter channels [5].

This brief literature review shows, that the heat transfer mechanism during flow boiling is still not sufficiently understood. A relationship between heat transfer coefficient and vapour quality varies with working fluids and experimental conditions. The aim of this work is to find a relationship between the heat transfer coefficient and the flow pattern in order to understand better the heat transfer mechanisms.

2. Set-up and experimental conditions

The experimental set-up for investigating thermofluid-dynamic phenomena in vertical microchannels is shown in Fig. 1. The main components of the flow loop are the fluid tank, the pump, the test section and the condenser. The flowmeter and the preheater are embedded in the pump. The test specimen is covered with a transparent plate (makrolon) to enable flow visualisation.

The de-ionised water (working fluid), fed by the pump, is preheated in the fluid tank and then heated up to the channel inlet temperature by the internal heater of the pump. In the channel the water is heated via the three channel walls. The two-phase mixture is condensed in the condenser and flows back to the fluid tank.

The rectangular channel is machined by conventional milling into the upper surface of a copper plate (Fig. 1). The mean width and depth of the channel is $W = 0.807$ mm, respectively $H = 0.346$ mm ($d_h = 0.48$ mm). The channel length is about $L = 330$ mm, with a heating length of 300 mm. The Confinement number Co^* for the investigated experimental conditions is greater than 0.5. So, according to the definition given by Kew

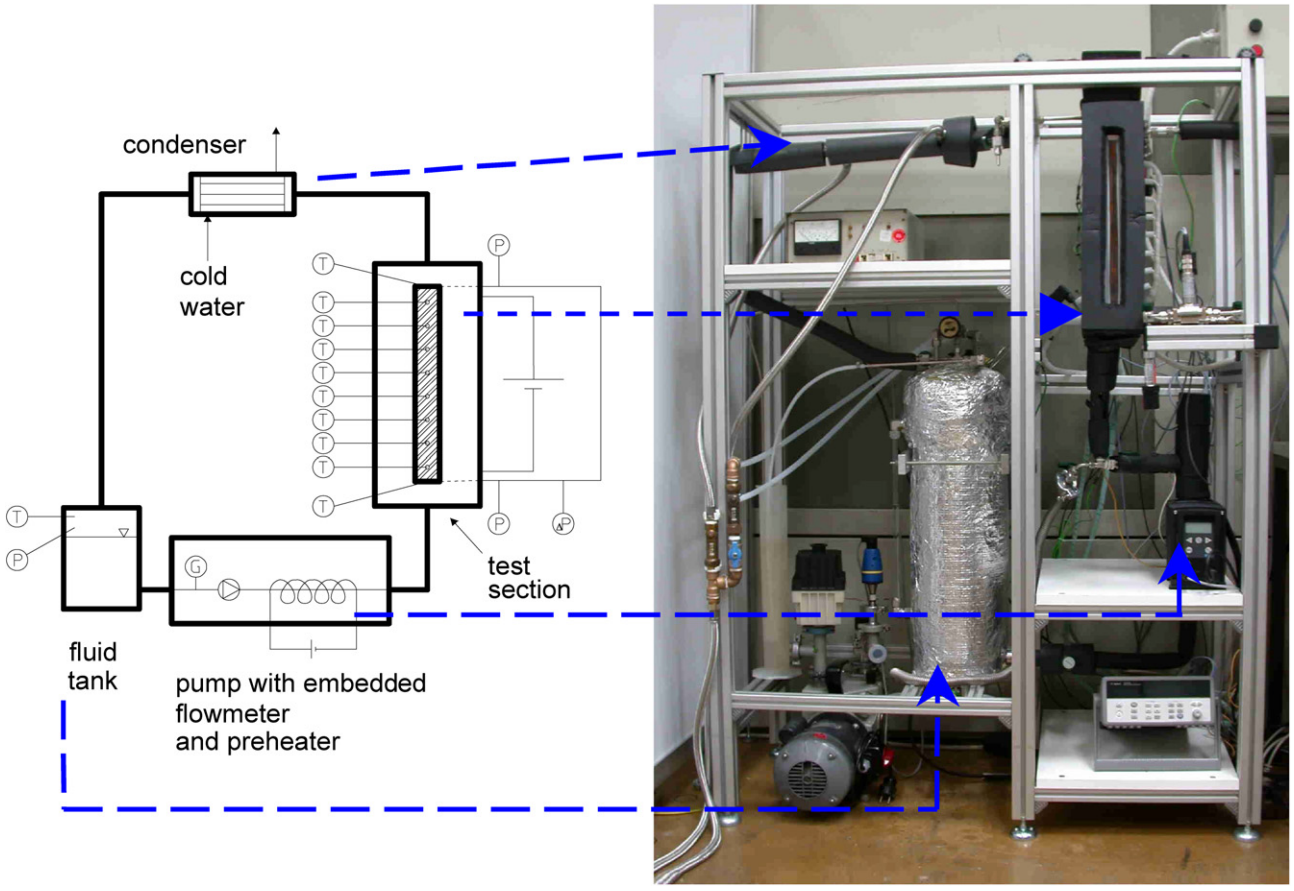

Fig. 1. Scheme of the test rig (left) and photograph of the experimental set-up (right).

and Cornwell [7], the tested channel has to be classified as narrow.

The test section consists of two main parts: 4 heater-blocks and the test specimen with the rectangular channel, all parts made from copper (Fig. 2). The flowing water in the channel is electrically heated by the heater-blocks from the back side of the test specimen. Based on the good thermal conductivity of the copper material and the very small channel dimension compared to the test specimen, it is reasonable to assume that the heat fluxes from the three channel sides are approximately equal.

The wall temperatures (Tw1–Tw8) are measured at eight positions along the channel on the backside of the test-specimen (position $Z = 47.5, 82.5, 123, 158, 198, 233, 273, 313$ mm from the channel inlet, Fig. 2). Flow patterns are observed at seven positions along the flow path corresponding to the thermocouple locations.

Four measurement parameters are determined:

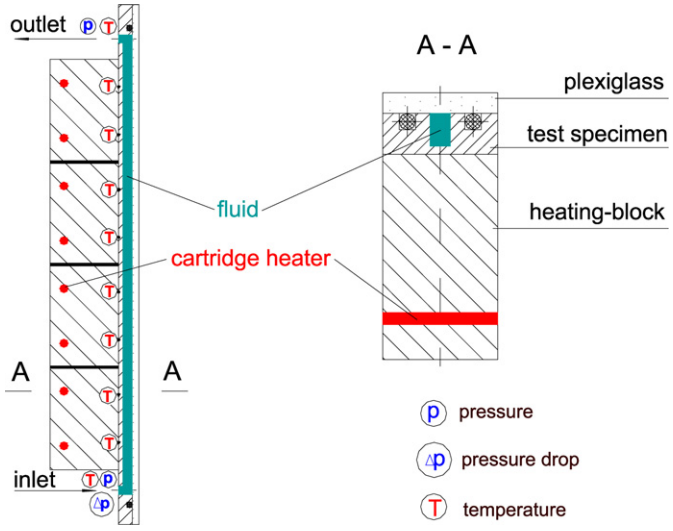

Fig. 2. Scheme of the test section.

1. Fluid temperatures at the inlet and outlet of the test section (PT-100, ±0.1 K) and wall temperatures at eight positions along the channel axis (thermocouples NiCr–Ni, type K, ±0.2 K).
2. Inlet and outlet fluid pressure (piezoresistive pressure transducers, ±500 Pa and ±200 Pa) and pressure drop between the inlet and outlet of the test section (two piezoresistive differential pressure transducers with different measurement ranges, ±500 Pa and ±200 Pa).
3. Input heating power (digital multimeter, ±1 W).
4. Mass flow rate of the working fluid (embedded in pump, ±0.06 g/min).

3. Data evaluation

3.1. Heat balance

The heat loss is mainly caused due to the convective heat transfer from the test section to the ambient. In order to determine the heat loss Q_{loss}, an energy balance is performed for single-phase flow, and the heat loss is estimated as a function of the wall temperature. Then the effective heat flux can be defined as

$$q = (Q - Q_{\text{loss}})/A \tag{1}$$

Due to the high pressure drop between the inlet and the outlet of a microchannel during flow boiling, the fluid pressure changes and hence, the corresponding change of the fluid saturation temperature along the channel cannot be neglected. The length Z_{sat} from the channel inlet, where the saturation condition starts, is calculated from the heat balance, Eq. (2).

$$G \cdot A_{\text{sect}} \cdot C_p(T_{L,\text{sat}} - T_{L,\text{in}}) = q \cdot S \cdot Z_{\text{sat}} \tag{2}$$

From former investigations it is well known that the two-phase flow starts already in a subcooled flow condition. Therefore, flow visualisation was used to define the position Z_{ONB} of the onset of boiling.

The pressure drop of the single-phase flow length is calculated with the Darcy–Weisbach equation and after subtraction from the inlet pressure this gives the pressure at positions Z_{sat} resp. Z_{ONB}. For two-phase flow, the assumption of a linear pressure drop was made. The two dot-dashed lines in Fig. 3 show the possible pressure profiles when the two-phase flow starts at Z_{sat}, respectively at Z_{ONB} (pressure drop at subcooled condition is also treated as a two-phase pressure drop). The mean values of these two profiles were taken as the final pressure profile of the two-phase flow regime. Thus, the pressure and fluid saturation temperature T_{sat} can be determined as a function of the position Z along the channel axis. The specific enthalpy of the liquid and the vapour at saturation under pressure $p(Z)$ is known. Based on the energy balance and the conservation of mass, the thermodynamic vapour quality x_{th} at position Z can be calculated. Eqs. (3)–(6) describe the liquid temperature T_L and the vapour quality x_{th} for an unsaturated and a saturated situation.

$$T_L(Z) = T_{L,\text{in}} + \frac{q \cdot S \cdot Z}{C_p \cdot G \cdot A_{\text{sect}}}, \quad Z < Z_{\text{sat}} \tag{3}$$

$$T_L(Z) = T_{\text{sat}}(p(Z)), \quad Z \geqslant Z_{\text{sat}} \tag{4}$$

$$x_{\text{th}}(Z) = \frac{(i_L(Z) - i_{L,\text{sat}})}{\Delta h_{\text{LG}}}, \quad Z < Z_{\text{sat}} \tag{5}$$

$$x_{\text{th}}(Z) = \frac{1}{\Delta h_{\text{LG}}}\left(\frac{q \cdot S \cdot Z}{G \cdot A_{\text{sect}}} + i_{L,\text{in}} - i_{L,\text{sat}}\right), \quad Z \geqslant Z_{\text{sat}} \tag{6}$$

3.2. Local heat transfer coefficient

With the assumption of a constant heat flux along the channel axis, the local heat transfer coefficient h_{TP} at position Z is given by Eq. (7). The liquid bulk temperature $T_L(Z)$ is calculated by Eq. (3) for an unsaturated flow regime or is taken as the local saturation temperature $T_{\text{sat}}(Z)$ corresponding to the local

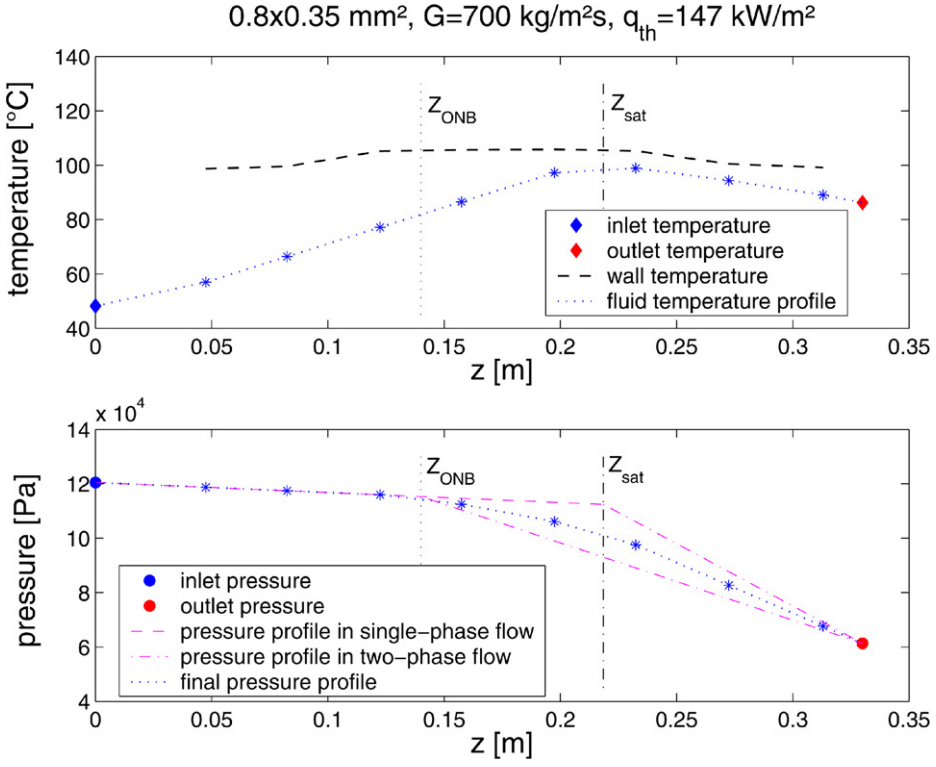

Fig. 3. Pressure and temperature profile along the channel length at $G = 700\ \text{kg m}^{-2}\ \text{s}^{-1}$ and $q = 147\ \text{kW m}^{-2}$.

saturation pressure. In addition thermodynamic equilibrium between the phases is assumed.

$$h_{\mathrm{TP}}(Z) = \frac{q}{T_w(Z) - T_L(Z)} \tag{7}$$

3.3. Flow pattern visualisation

Usually bubbly, slug, churn and annular flow occur in vertical conventional size channels during upward two-phase flow. There can be also some mixed types like wispy-annular or mist flow. In small-diameter channels different forces become dominant which influence the flow patterns. In the literature synonyms of flow pattern names coexist. Cornwell and Kew [8] found in multichannels with hydraulic diameters less than 1.7 mm isolated bubbles, confined bubbles and annular-slug flow. Nucleate boiling with isolated bubbles, nucleate boiling with coalesced bubbles and partial dryout regimes in a narrow vertical gap were reported by Bonjour and Lallemand [9]. For an air–water and steam–water flow in horizontal tubes, Feng and Serizawa [10] distinguished dispersed bubbly flow, gas slug flow, liquid ring flow and liquid lump flow. During boiling of water in a single rectangular channel with $d_h = 0.333$ mm different flow patterns were observed by Balasubramanian and Kandlikar [11], viz. nucleate boiling, slug formation, dryout, reverse flow and two-phase flow at the exit manifold. Vlasie's et al. [5] review about boiling behaviour of refrigerants found that three flow pattern names are commonly used in the literature: isolated bubble, confined bubble and annular flow.

The velocity of a vapour body is calculated as a length of the channel part inside the view window (about 3 mm of channel length is visualised) divided by the time which the vapour–liquid interface (top and bottom of vapour body) needs to pass through it. Considering the flow direction, the velocities of the top and bottom of the vapour body were calculated.

3.4. Flow pattern maps

A lot of flow pattern maps are presented in the literature. The first flow pattern map for a horizontal channel was presented by Baker [12,13] and modified by Scott [14]. Hewitt and Roberts [15] proposed one of the first flow pattern maps for vertical tubes. They distinguished bubbly, bubbly-slug, slug, churn, wispy-annular and annular flow. The investigations were undertaken on low-pressure air–water and high-pressure steam–water flows in small diameter tubes (10–30 mm).

Taitel et al. [16] presented a flow pattern map with superficial gas and liquid velocities based on experimental results obtained from vertical pipes (diameter 20–60 mm) with an air–water flow. They suggested physical mechanisms for each flow transition where the transition boundaries separate bubbly, dispersed bubbly, slug, churn and annular flow.

According to the Taitel et al. model, the slug flow requires a process of bubble agglomeration or coalescence which occurs when the void fraction α is high enough (e.g. $0.25 \leqslant \alpha \leqslant 0.3$). For the calculation of the bubbly-slug transition boundary, $\alpha = 0.25$ was considered. Finally, this transition boundary, respectively the corresponding liquid superficial velocity j_L is described by Eq. (8).

$$j_L = 3.0 \cdot j_G - 1.15\left(\frac{\sigma g(\rho_L - \rho_G)}{\rho_L^2}\right)^{0.25} \tag{8}$$

Annular flow cannot exist unless the gas velocity in the gas core is not sufficient to lift the entrained droplets. Eq. (9) predicts the minimum value of the superficial gas velocity j_G needed for a stable annular flow.

$$\frac{j_G \rho_G^{0.5}}{(\sigma g(\rho_L - \rho_G))^{0.25}} = 3.1 \tag{9}$$

Similar flow pattern maps, also for vertical tubes but with different transition criteria, were reported by Mishima and Ishii [17]. They postulated that flow parameters such as void fraction are conceptually simpler and therefore more reliable to predict flow pattern boundaries.

The Mishima–Ishii model, based on the same fundamentals as the Taitel et al. model, assumes a void fraction $\alpha = 0.3$ for the bubbly-slug transition boundary. With this assumption and the relationship between the superficial velocities derived from the drift velocity for bubbly flow (Ishii [18]), the bubbly-slug boundary is described by Eq. (10).

$$j_L = \left(\frac{3.33}{C_0} - 1\right) j_G - \frac{0.76}{C_0}\left(\frac{\sigma g(\rho_L - \rho_G)}{\rho_L^2}\right)^{0.25} \tag{10}$$

where the distribution parameter C_0 for rectangular ducts is given by Eq. (11).

$$C_0 = 1.35 - 0.35\sqrt{\frac{\rho_G}{\rho_L}} \tag{11}$$

Furthermore, the Mishima–Ishii model contains two criteria for the churn-annular boundary which are used to describe the slug-annular transition. For small diameter channels, Eq. (12) is proposed, for large channels, Eq. (13) is applicable.

$$j_G = \sqrt{\left(\frac{g d_h(\rho_L - \rho_G)}{\rho_G}\right)}(\alpha - 0.11) \tag{12}$$

$$j_G \geqslant \left(\frac{\sigma g(\rho_L - \rho_G)}{\rho_G^2}\right)^{0.25} \cdot N_{\mu L}^{-0.2} \tag{13}$$

The boundary channel diameter is defined by Eq. (14).

$$d = \frac{\sqrt{\frac{\sigma}{g(\rho_L - \rho_G)}} N_{\mu L}^{-0.4}}{(\frac{1 - 0.011 C_0}{C_0})^2} \tag{14}$$

where the viscosity number $N_{\mu L}$ (see also Eq. (13)) can be approximately calculated with

$$N_{\mu L} \cong \frac{\mu_L}{(\rho_L \sigma \sqrt{\frac{\sigma}{g(\rho_L - \rho_G)}})^{0.5}} \tag{15}$$

Other flow pattern maps were proposed by Lin et al. [19] for vertical small tubes and by Tabatabai and Faghri [20] for horizontal miniature and micro tubes. In [19] two dimensionless parameters, the Confinement and Kutateladze number, were introduced. In [20] the importance of the surface tension for two-phase flows in horizontal channels was emphasised.

For diabatic horizontal flows, a boiling transition boundary criterion has been proposed by Zürcher et al. [21]. Because of different flow patterns compared to vertical flows, only the intermittent to annular flow transition is useful. According to the authors the intermittent flow pattern occurs at a low vapour quality and groups unsteady flow patterns like plug and slug flow. They proposed, following Steiner [22], a criterion based on the Martinelli parameter, Eq. (16).

$$X_{\mathrm{tt}} = \left(\frac{\mu_L}{\mu_G}\right)^{0.125} \left(\frac{1-x_{\mathrm{th}}}{x_{\mathrm{th}}}\right)^{0.875} \left(\frac{\rho_G}{\rho_L}\right)^{0.5} = 0.34 \tag{16}$$

The gas and liquid superficial velocities, Eqs. (17) and (18), are needed to establish flow pattern maps for comparing flow regimes of different channel geometries.

$$j_G = \frac{V_G}{A_{\mathrm{sect}}} = \frac{G \cdot x_{\mathrm{th}}}{\rho_G} \tag{17}$$

$$j_L = \frac{V_L}{A_{\mathrm{sect}}} = \frac{G(1-x_{\mathrm{th}})}{\rho_L} \tag{18}$$

4. Experimental results and discussion

4.1. Flow pattern visualisation

In order to eliminate the confusion about the flow pattern terminology, only 3 basic flow patterns are distinguished in following discussion: bubbly, slug and annular flow. Because of the test section's construction only a two-dimensional visualisation can be done. Hence, some assumptions related to the third dimension have to be made. Three categories of observed vapour bodies were distinguished, Fig. 4. At this point it must be emphasised that the depth of the channel ($H = 0.346$ mm) is smaller than its width ($W = 0.807$ mm). In the first category there are spherical bubbles with diameters smaller than the depth of the channel, Fig. 4a. In the second category the observed vapour bodies have diameters between 0.346 and 0.807 mm what gives an appearance of round bubble shapes but because of the lower channel depth, they are not perfect spheres, Fig. 4b. Vapour bodies with a length greater than the channel width belong to the third category. The cross-section of these slugs is assumed to be elliptical, Fig. 4c.

For bubbly flow, the gas phase (isolated bubbles) is moving in the continuous liquid phase. If there is a majority of vapour bodies from the first and the second category, then it is bubbly flow.

For slug flow, Taylor bubbles are typical. The diameters of these bubbles are close to the channel diameter, and they have usually a round front-side and flat back-side shape. They belong to the third category.

For annular flow, the gas phase is moving in the core of the channel, and the liquid phase is in an annulus along the wall. In present visualisation experiments a typical annular flow was not observed. There were always some liquid bridges which cause interrupts of the annular flow. Such type of flow can be treated as a flow with very long slugs (third category). Hence, the boundary between slug and annular flow is introduced on the basis of slug lengths, i.e. a flow with slugs longer than hundred times of the channel width is called annular flow.

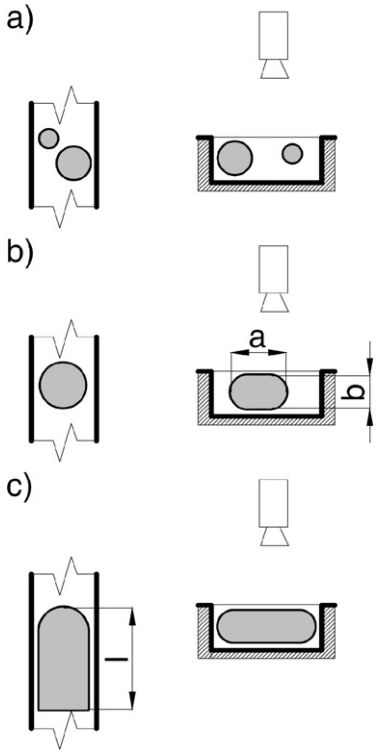

Fig. 4. Classification of observed vapour bodies into three categories.

At every thermocouple position along the channel axis the two-phase flow was observed and high-speed videos were recorded, usually twice with two different recording frequencies. In this context it should be mentioned that there were hardly image sequences containing only vapour bodies of one category. Hence, size distributions of vapour body lengths (histograms) were established by means of image analyses in order to define flow patterns. To emphasise a variety of the term "slug", all slugs were subclassified into three groups with different lengths but all belonging to the slug flow regime.

By means of the histograms for mass fluxes 1500 kg m^{-2} s^{-1} and 131 kW m^{-2}, Fig. 5, the procedure to fix a flow regime at a certain channel position can be explained as follows: At three thermocouple positions (Tw6, Tw7 and Tw8) bubbles and short slugs were observed. Because of the majority of bubbles (about 70%) at Tw6-position there is bubbly flow defined. At Tw7- and Tw8-position 66% of observed vapour bodies were slugs with different lengths greater than 0.81 mm, and hence there is per definition slug flow.

It should be pointed out that a wide flow range can be named slug flow. For mass flux 1500 kg m^{-2} s^{-1} and 131 kW m^{-2} at Tw8-position for instance, slug flow was defined, even though a large amount of bubbles was observed. A different kind of slug flow was found for mass fluxes 200 kg m^{-2} s^{-1} and 110 kW m^{-2} at Tw3-position where very long slugs exist likewise an annular flow pattern.

4.2. Local heat transfer coefficient

Fig. 6 presents local heat transfer coefficients vs. thermodynamic vapour qualities for mass fluxes 200, 700 and

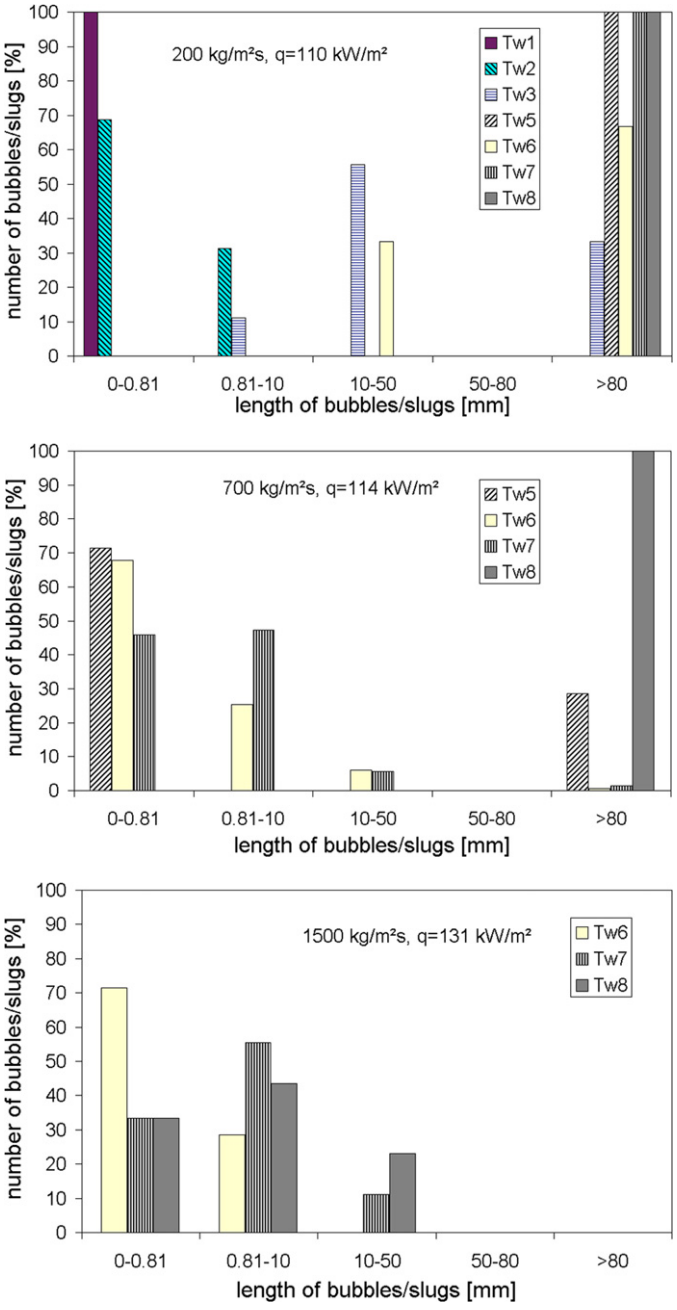

Fig. 5. Histograms of vapour body length for mass fluxes 200 (a), 700 (b) and 1500 (c) kg m^{-2} s^{-1} and heat flux of about 115 kW m^{-2}.

1500 kg m^{-2} s^{-1}. The two dashed lines show roughly the boundary transitions. The two-phase flow starts at negative vapour quality at all considered mass fluxes.

For the smallest mass flux, bubbles were observed from the first thermocouple position. For higher mass fluxes, even for higher heat fluxes, single-phase flow was observed at an initial length (boiling was not initiated there). It should be emphasised that the experiments were performed always under subcooled condition at the channel inlet to guarantee liquid flow there. The growth of bubbles and their agglomerations change the flow pattern from bubbly to slug flow and as things developed, to annular flow. A partial dryout close to the

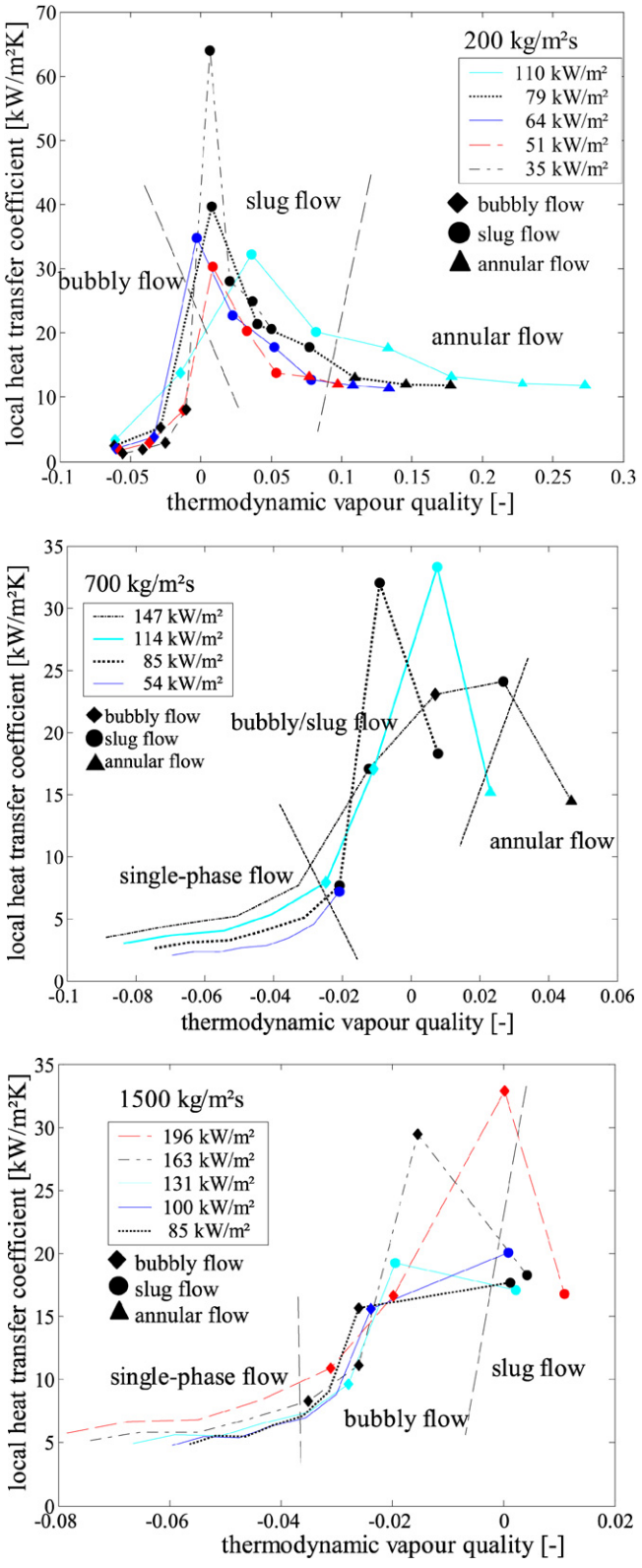

Fig. 6. Local heat transfer coefficients for mass fluxes 200 (a), 700 (b) and 1500 (c) kg m^{-2} s^{-1}.

channel outlet was also observed, especially for the mass flux 200 kg m^{-2}s^{-1}.

The local heat transfer coefficient has a maximum for slug flow at mass flux 200 kg m^{-2} s^{-1} and 700 kg m^{-2} s^{-1}, and for

bubbly flow at mass flux 1500 kg m^{-2} s^{-1}. Usually such maxima were observed at thermodynamic vapour qualities close to zero and in a short distance to the onset of boiling. Hence, it can be pointed out that nucleate boiling is dominant at these positions. With the elongation of bubbles and slugs convective boiling becomes a considerable heat transfer mechanism. A thinning of the liquid layer by evaporation can provide locally and temporary dried areas. This mechanism causes a decrease of local heat transfer coefficients along the channel.

In the literature it is commonly assumed that nucleate boiling is dominant when the heat transfer coefficient is increasing with the heat flux. On the other hand convective boiling is dominant when the heat transfer coefficient increases with increasing mass flux and vapour quality. In Fig. 6 the local heat transfer coefficient rises with the heat flux (this holds especially for mass flux 200 kg m^{-2} s^{-1} under saturated condition) what could indicate nucleate boiling. However, from flow observations at corresponding positions (slug and annular flow) one would expect a convective boiling.

It is remarkable that the local heat transfer coefficient at mass flux 200 kg m^{-2} s^{-1}, respectively 35 kW m^{-2} and a vapour quality close to zero is greater than for higher heat fluxes. This may be a consequence of the assumptions for the pressure/temperature profile calculations (see Section 3) what affects the local heat transfer coefficient. Because of no available local pressure data along the channel, a pressure profile had to be assumed. Therefore, the start position of the two-phase flow corresponds sometimes not exactly to the assumed position. This induces an increased artificial pressure, and in consequence a higher temperature which results in an increase of the calculated heat transfer coefficient.

It is noticeable that for the mass flux 700 kg m^{-2} s^{-1} at heat fluxes 114 kW m^{-2} and 147 kW m^{-2} bubbly flow was observed at Tw5- and Tw6-position, respectively Tw5-position (see Fig. 6). That does not mean that no bubbles occur at other heat fluxes and channel positions. From the histogram data it is clear, there are more slugs than bubbles. Apart from the type of the two-phase flow—bubbles and/or slugs, also their frequency of occurrence has to be considered. The Tw6-position at imposed heat fluxes 147, 114 and 85 kW m^{-2} will be taken as an example (Table 1): For the highest heat flux 147 kW m^{-2}, 115 counts of vapour bodies were observed in the length range 0–0.81 mm, corresponding to 81% of the total count. For heat flux 114 kW m^{-2}, a large number of vapour bodies occurs in the length range 0–0.81 mm (201 counts to total count 296, i.e. 68%). Only 33 vapour bodies were observed at heat flux 85 kW m^{-2}, therein 13 bubbles and 20 short slugs. For lower heat fluxes, no two-phase flow is at Tw6-position. Considering the recording times at this position local bubble/slug passing through frequencies of 312, 186 and 21 s^{-1} can be determined.

In Fig. 7 the velocities of the vapour body tops and bottoms are shown. Due to the slug growth elongating the vapour bodies, the top-velocities are as a rule higher than the bottom-velocities. With decreasing vapour body size the velocity differences become smaller. The solid vertical lines in the diagram represent the boundaries between different vapour body length groups.

Table 1
Distribution of bubbles/slugs at Tw6-position for mass flux 700 kg m^{-2} s^{-1} and different heat fluxes

Length [mm]	Heat flux [kW m^{-2}]		
	147	114	85
0–0.81	115	201	13
0.81–10	23	75	20
10–50	1	18	0
50–80	0	0	0
>80	3	2	0
total number	142	296	33
recording time [s]	0.455	1.591	1.591
frequency of bubble/slug passing through [s^{-1}]	312	186	21

4.3. Flow pattern map

The flow pattern map in Fig. 8 shows a dominant bubbly flow for negative vapour qualities. The bubbly-slug transition is at a vapour quality of about $x_{\text{th}} \approx -0.01$. Annular flow was observed only under saturated flow conditions and starts at a low vapour quality ($x_{\text{th}} \approx 0.05$). Some of the transition boundaries from the literature are shown as vertical lines. The superficial velocities proposed as boundaries were rearranged into boundary of vapour quality according to Eqs. (17) and (18).

The slug-annular transition is described by the Mishima–Ishii model (criterion for large channels) as well as by the Taitel model (dotted line) quite well.

Mishima and Ishii [17] used their model criteria also for comparison with experimental data from a steam–water flow in a rectangular channel $d_h = 5.64$ mm at high pressure (Hosler [23]). The comparison showed reasonable agreement. In our case, the most probable reason for the differences between the theory and the experimental results is the variant inlet pressure which is smaller for the presented experiments. The assumption that the void fraction during bubbly-slug transition is $\alpha = 0.3$ can also be an additional reason. However, the criterion for the churn-annular flow transition (dash-dotted line) describes the experimental data very well.

Taitel et al. [16] compared their model criteria with experimental data from a air–water flow in pipes with $d_h = 20$–60 mm at low pressure. The proposed churn-annular criterion (dotted line) works quite well for our case. Different channel hydraulic diameters cause various forms of bubbly flow. For channels in centimetre-scales, a lot of small isolated bubbles can be expected, while in narrow channels bubbles reach very quickly a diameter comparable to the channel size. In consequence for the bubbly-slug boundary, the void fraction assumption $\alpha = 0.25$ can be a reason for the large discrepancy to the experimental data.

The intermittent-annular criterion proposed by Zürcher et al. [21], Eq. (16), was calculated for 90 °C. As can be seen from Fig. 8, this criterion cannot describe the experimental slug-annular transition.

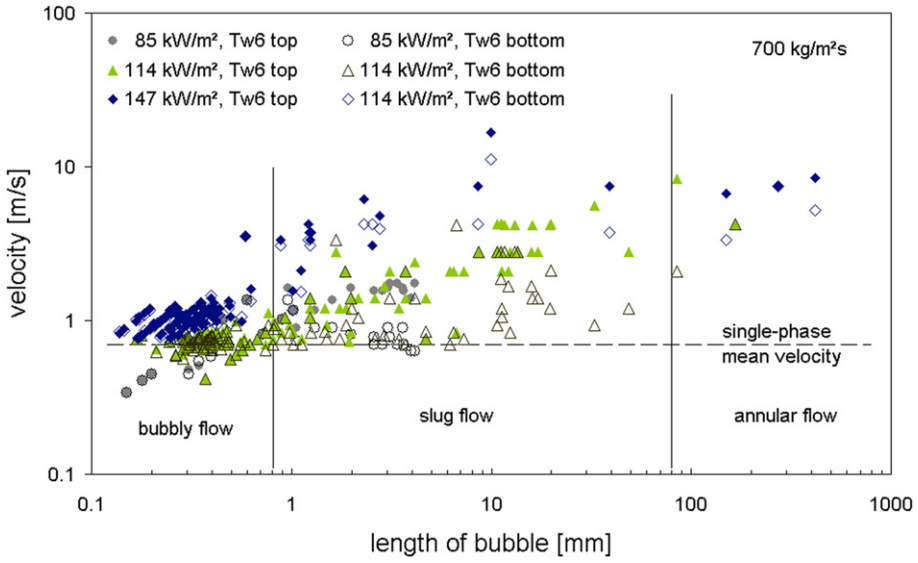

Fig. 7. Bubble and slug velocities.

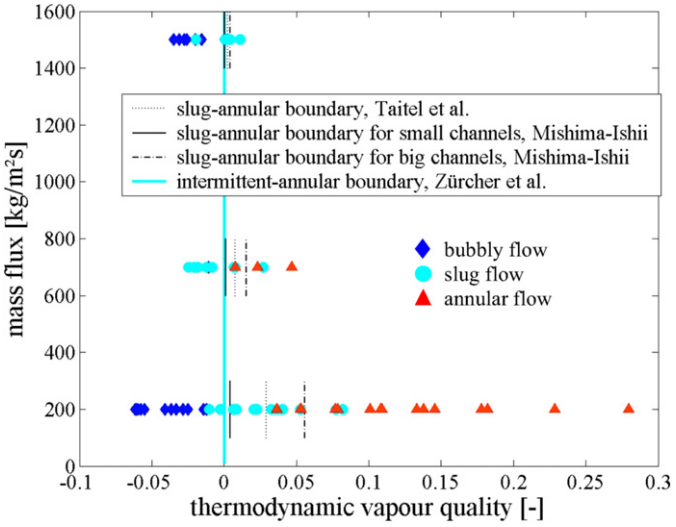

Fig. 8. Flow pattern map for the vertical rectangular narrow channel.

5. Conclusions

Experimental results for flow boiling of water in a vertical rectangular channel (width × depth = 0.807 × 0.346 mm^2, d_h = 0.48 mm) are presented including two-phase flow heat transfer coefficients, flow patterns and the relationship between them.

The following main results have been found:

– The heat transfer coefficient at the channel inlet increases very slightly because of the subcooled single-phase flow. Near to the onset of boiling the nucleation mechanism usually dominates, and there is a maximum of the heat transfer coefficient. Bubbly flow or slug flow (with relatively short slugs) is observed at this position. With increasing vapour quality the flow regime undergoes a transition to an annular flow. Then the film vaporisation (convective boiling) becomes a considerable heat transfer mechanism and can even completely suppress the nucleate boiling. Furthermore, the liquid film may completely disappear (dryout) or only at some channel positions (local partial dryout). As a result the heat transfer coefficient increases channel upwards until to a certain position. Because the local dried areas are relatively inactive, the heat transfer coefficient (average value around the channel perimeter) decreases continuously with the decrease of wetted parts of the channel wall. It can be concluded that in narrow space channels nucleate boiling is a most effective heat transfer mechanism. In comparison with conventional size channels, where convective boiling during annular flow offers the best heat transfer performance, the maximum of the heat transfer performance is shifted towards the inlet of the channel.

– By means of flow visualisation three main basic flow patterns can be found: bubbly, slug and annular flow. It should be pointed out that often different vapour body formations occur simultaneously for one imposed mass and heat flux, e.g. bubbles were observed after slugs at the same channel position. In such cases a main flow pattern was defined due to the individual corresponding dominance. Based on flow visualisations a first attempt was carried out for classifying the vapour body shape and length. Moreover, size distributions of the vapour body length were determined at different channel positions for three mass fluxes (200, 700 and 1500 kg m^{-2} s^{-1}) and different heat fluxes. In addition local frequencies of classified vapour bodies were specified considering the range of experimental conditions.

– The comparison between the established flow pattern map and existing models from the literature shows that the experimentally found slug-annular transition is described by the Mishima–Ishii model (criterion for large channels) and the Taitel model quite well.

Acknowledgement

Ms. Ewelina Sobierska acknowledges the financial support provided by the European Community's Human Potential Programme under contract HPRN-CT-2002-00204, HMTMIC.

References

[1] P. Van Carey, Liquid–Vapor Phase Change Phenomena, Taylor and Francis, 1992.
[2] M.C. Diaz, H. Boye, I. Hapke, J. Schmidt, Y. Staate, Z. Zhekov, Flow boiling in mini and microchannel, in: S.G. Kandlikar (Ed.), Proc. 2nd Int. Conf. on Microchannels and Minichannels, Rochester, New York, ISBN 0-7918-4164-2, 2004, pp. 445–452.
[3] S. Lin, P.A. Kew, K. Cornwell, Two-phase heat transfer to a refrigerant in a 1 mm diameter tube, Int. J. Refrigeration 24 (2001) 51–56.
[4] B. Agostini, A. Bontemps, Vertical flow boiling of refrigerant R134a in small channels, Int. J. Heat Fluid Flow 26 (2004) 296–306.
[5] C. Vlasie, H. Macchi, J. Guilpart, B. Agostini, Flow boiling in small diameter channels, Int. J. Refrigeration 27 (2004) 191–201.
[6] T.N. Tran, M.W. Wambsganss, D.M. France, Small circular- and rectangular-channel boiling with two refrigerants, Int. J. Multiphase Flow 22 (3) (1996) 485–498.
[7] P.A. Kew, K. Cornwell, Confined bubble flow and boiling in narrow spaces, in: Proc. 10th Int. Heat Transfer Conf., Brighton, vol. 7, 1994, pp. 473–478.
[8] K. Cornwell, P.A. Kew, Boiling in small parallel channels, in: Proc. CEC Conf. on Energy Efficiency in Process Technology, Athens, October 1992, Paper 22, Elsevier Applied Sciences, 1992.
[9] J. Bonjour, M. Lallemand, Flow patterns during boiling in a narrow space between two vertical surfaces, Int. J. Multiphase Flow 24 (1998) 947–960.
[10] Z. Feng, A. Serizawa, Two-phase flow patterns in ultra-small-channels, in: 2nd Japanese–European Two-Phase Flow Meeting, Tsukuba, September 25–29, 2000.
[11] P. Balasubramanian, S.G. Kandlikar, High speed photographic observation of flow patterns during flow boiling in single rectangular minichannel, in: Proc. HT2003, ASME Summer Heat Transfer Conf., Las Vegas, Nevada, USA, July 21–23, 2003.
[12] O. Baker, Simultaneous flow of oil and gas, Oil Gas J. 53 (1954) 185–190.
[13] O. Baker, Designing Pipelines for Simultaneous Flow of Oil and Gas, Handbook Section, Pipeline Engineering, PH, 1960.
[14] D.S. Scott, Properties of Co-Current Gas–Liquid Flow, Advances in Chemical Engineering, vol. 4, Academic Press, New York, 1963, 199.
[15] G.F. Hewitt, D.N. Roberts, Studies of two-phase flow patterns by simultaneous X-ray and flash photography, AERE-M 2159, HMSO, 1969.
[16] Y. Taitel, D. Bornea, A.E. Duckler, Modelling flow pattern transitions for steady upward gas–liquid flow in vertical tubes, AIChE J. 26 (3) (1980) 345–354.
[17] K. Mishima, M. Ishii, Flow regime transition criteria for upward two-phase flow in vertical tubes, J. Heat Mass Transfer 27 (5) (1984) 723–736.
[18] M. Ishii, One-dimensional drift-flux model and constitutive equations for relative motion between phases in various two-phase flow regimes, ANL Report ANL-77-47, 1977.
[19] S. Lin, P.A. Kew, K. Cornwell, Characteristic of air/water flow in small tubes, Heat and Technology, Calore e Tecnologia 17 (2) (1999) 63–70.
[20] A. Tabatabai, A. Faghri, A new two-phase flow map and transition boundary accounting for surface tension effects in horizontal miniature and micro tubes, J. Heat Transfer 123 (2001) 958–968.
[21] O. Zürcher, D. Favrat, J.R. Thome, Development of a diabatic two-phase flow pattern map for horizontal flow boiling, Int. J. Heat Mass Transfer 45 (2) (2002) 291–301.
[22] D. Steiner, VDI-Wärmeatlas (VDI Heat Atlas), VDI-Gesellschaft Verfahrenstechnik u. Chemieingenieurwesen (GCV), Translator: J.W. Fullarton, Chapter Hbb., Düsseldorf, 1993.
[23] E.R. Hosler, Flow patterns in high pressure two-phase (steam–water) flow with heat addition, Chem. Engrg. Prog. Symp. Ser. 64 (82) (1968) 54.